Ultrasonic and neutron diffraction studies of dilute Cr-Re and Cr-Ru alloy single crystals

1993 J. Phys.: Condens. Matter 5 5353

(http://iopscience.iop.org/0953-8984/5/30/015)

J. Phys.: Condens. Matter 5 (1993) 5353–5370. Printed in the UK

Ultrasonic and neutron diffraction studies of dilute Cr–Re and Cr–Ru alloy single crystals

A H Boshoff, H L Alberts, P de V du Plessis and A M Venter†
Department of Physics, Rand Afrikaans University, PO Box 524, Aucklandpark 2006, South Africa

Received 7 April 1993

Abstract. Measurements are reported on the temperature dependence of the elastic constants of dilute Cr–Ru and Cr–Re alloy single crystals, containing respectively 0.3 at.% Ru, 0.5 at.% Ru, 0.3 at.% Re and 0.5 at.% Re. Neutron diffraction experiments were also performed on the two Cr–Ru crystals. Well defined anomalies were observed in all the elastic constants as well as in the integrated neutron intensities at the magnetic phase transitions of the alloys. The commensurate (C) spin density wave (SDW) to paramagnetic (P) and incommensurate (I) SDW to P transitions are second-order phase transitions, while the ISDW–CSDW and CSDW–ISDW transitions are of first order. A thermodynamic model describes the temperature dependence of the magnetic contributions (ΔB) to the bulk modulus (B) reasonably well, but fails to give the observed relationship between ΔB and the magnetization.

1. Introduction

The binary systems of Cr alloys with group 7 and group 8 non-magnetic transition metal elements, Re and Ru respectively, have very similar magnetic phase diagrams [1]. They are both itinerant electron spin density wave (SDW) antiferromagnetic systems in which the magnetic moment, $\mu(r)$, is sinusoidally modulated along a cubic axis with a modulation vector Q given by $Q = (2\pi/a)(1 - \delta)$, where a is the lattice parameter and δ is known as the incommensurability factor. Three magnetic phases appear on the magnetic phase diagrams of Cr–Re and Cr–Ru alloys: an incommensurate (I) SDW phase with $\delta \neq 0$, a commensurate (C) SDW phase with $\delta = 0$ and the paramagnetic (P) phase [1]. For both systems a triple point exists below 0.5 at.% solute where these three phases co-exist and in both the SDW phase persists up to high (~ 20 at.%) Re or Ru concentrations [1]. There is a peak in the C–P phase boundary line for both near 575 K at concentrations of about 7 at.% Re or 3 at.% Ru, respectively.

The magnetic behaviour of Cr alloys in the vicinity of the triple point is of particular interest, as alloys near this point exhibit the largest number of magnetic phases that can be present in a single Cr alloy. Except for some single-crystal neutron diffraction studies on Cr–Re [2–4], nearly all previous studies on magnetic effects in dilute Cr–Re and Cr–Ru alloys were done on polycrystalline material. These studies are thus of limited value in gaining an insight into the magnetic effects of the two alloy systems. This is particularly so for magnetoelastic effects for which polycrystalline measurements give incomplete information concerning the effects of the SDW on the elastic properties. Recently, we reported an initial

† Department of Materials Technology, Atomic Energy Corporation of South Africa (Ltd), PO Box 582, Pretoria 0001, South Africa.

0953-8984/93/305353+18$07.50

study of the magnetoelastic behaviour of a Cr + 0.3 at.% Ru single crystal [5] and observed anomalies in all single-crystal elastic constants at the I–C transition temperature T_{IC}. This alloy shows strong longitudinal magnetoelastic effects and is unique in also showing strong shear effects in the CSDW phase [1]. A microscopic theory is presently not available to explain this unique behaviour and single-crystal elastic constant measurements on other Cr–Ru alloys, as well as on Cr–Re alloys with the same type of magnetic phase diagram, should give valuable information needed in developing such a theory.

We report here a detailed study of the temperature dependence of the elastic constants of Cr–Re and Cr–Ru alloy single crystals with concentrations in the vicinity of the triple point. Neutron diffraction measurements were also made on the Cr–Ru crystals. The elastic neutron scattering experiments enabled an experimental determination of the relationships between the magnetic contributions to the bulk modulus and the SDW magnetic moment as well as between the magnetovolume and this moment. Relationships between these physical quantities are expected [1] from simple thermodynamic models and the neutron measurements serve to check the predicted equations. The neutron studies furthermore give information on the order of the transitions at T_{IC} and at the Néel point T_N. In earlier work the order of the transition and a check for hysteresis effects at the transitions were not investigated because of inhomogeneities in the Cr–Re crystal used [3] or due to the fact that a powder was used in the Cr–Ru measurements [6]. As far as we are aware the present study is the first report on single-crystal neutron diffraction of dilute Cr–Ru alloys.

2. Experimental techniques

Single crystals of Cr–Re and Cr–Ru alloys of nominal concentrations 0.3 at.% Re, 0.5 at.% Re, 0.3 at.% Ru and 0.5 at.% Ru were grown by a floating-zone technique using RF heating. The starting materials were 99.996% Iochrome (trade name of Materials Research Corporation, Orangeburg, USA), 99.9% Re and 99.9% Ru. Electron microprobe analyses at different positions on the crystals show that they are fairly homogeneous with actual concentrations of (0.25 ± 0.03) at.% Re, (0.47 ± 0.04) at.% Re, (0.28 ± 0.02) at.% Ru and (0.43 ± 0.03) at.% Ru respectively. The crystals were prepared by spark planing parallel (110) and in some cases also parallel (100) faces, the latter for internal consistency checks of the elastic constants. The distance between both sets of parallel faces was approximately 5–6 mm while the surface areas were of the order of 20 mm^2.

The experimental techniques for velocity of sound measurements are described elsewhere [7]. Ultrasonic (10 MHz) pulse transit times were measured while slowly heating the sample from low to high temperatures at a rate of about 0.6 K per minute. Hysteresis effects were not checked during the ultrasonic measurements on the Cr–Ru crystals, it was instead studied during the neutron measurements on these crystals. In the case of the Cr–Re crystals, ultrasonic measurements were, however, also performed for the Cr + 0.5 at.% Re crystal during the cooling cycle in order to check for hysteresis effects at T_{IC}. The experimental error in the absolute values of sound velocity amounts to 0.5%, while changes of 1 in 10^3 with temperature could be detected easily. All measurements were performed on the as-grown crystals. In calculating the elastic constants from the measured wave velocities, densities determined from the lattice parameters [8,9] of the alloys were used. The wave velocity measurements were done in the temperature range 4–500 K.

Neutron diffraction experiments were only performed on the two Cr–Ru crystals due to limited neutron beam time. Since Cr–Ru and Cr–Re systems have similar magnetic phase diagrams, this limitation should not invalidate the general conclusions of this study.

Elastic scattering experiments were performed using neutrons of wavelength $\lambda = 1.07$ Å and with a $\lambda/2$ contamination of less that 0.3% as selected with a Ge(111) monochromator from the thermal beam of the nuclear reactor at Pelindaba, Pretoria. Magnetization values characterizing the SDW were obtained from integrated intensity scans through magnetic peaks as described in subsection 3.2.1. Employing the low-temperature equipment described previously [10], temperatures in the range 12–300 K were attainable and regulated stable to within ±0.02 K during individual scans. A furnace previously used by Greenwood and du Plessis [11] for neutron diffraction measurements, was employed in the temperature range 300–500 K rendering temperature stability of ±0.04 K. Measurements were performed during both heating and cooling runs. Neutron measurements were made against a preselected monitor count sampled by a monitor counter placed in the incoming neutron beam to account for changes in reactor power.

3. Results

3.1. Elastic constants

The temperature dependence of c_{11}, c_{44}, $\frac{1}{2}(c_{11} - c_{12})$ and $c_L = \frac{1}{2}(c_{11} + c_{12} + 2c_{44})$ for the Cr–Ru and Cr–Re crystals are shown in figures 1–4.

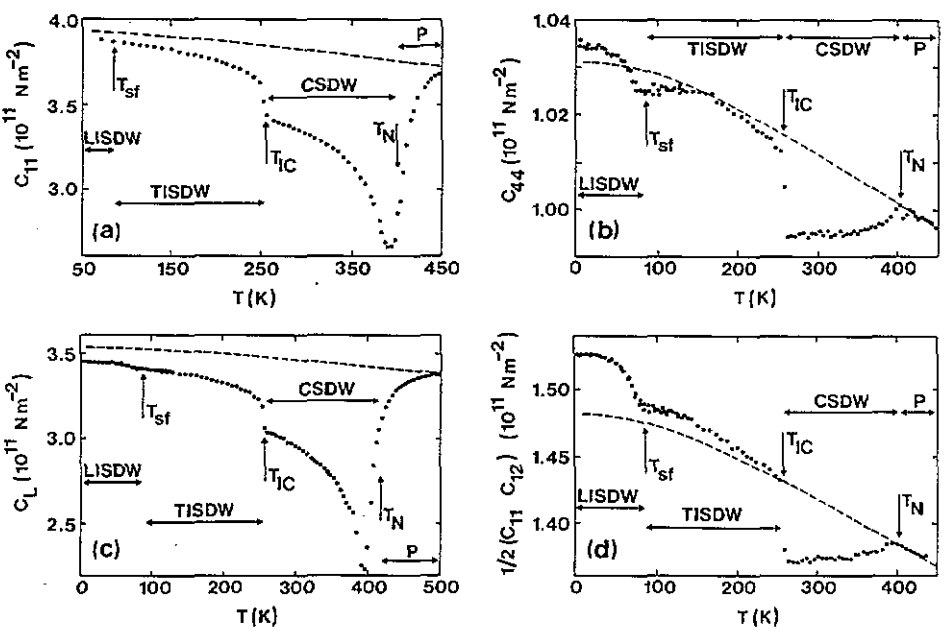

Figure 1. The temperature dependences of the elastic constants of Cr + 0.3 at.% Ru are depicted by points: (*a*) c_{11}, (*b*) c_{44}, (*c*) $c_L = \frac{1}{2}(c_{11} + c_{12} + 2c_{44})$ and (*d*) $\frac{1}{2}(c_{11} - c_{12})$. Only every eighth measured point is plotted for clarity. The broken curves represent the non-magnetic behaviour obtained from the temperature dependence of the corresponding elastic constant of a Cr + 5 at.% V crystal.

Three anomalies were observed in the temperature dependence of the elastic constants of Cr + 0.3 at.% Ru and Cr + 0.5 at.% Re (figures 1 and 4). According to the magnetic

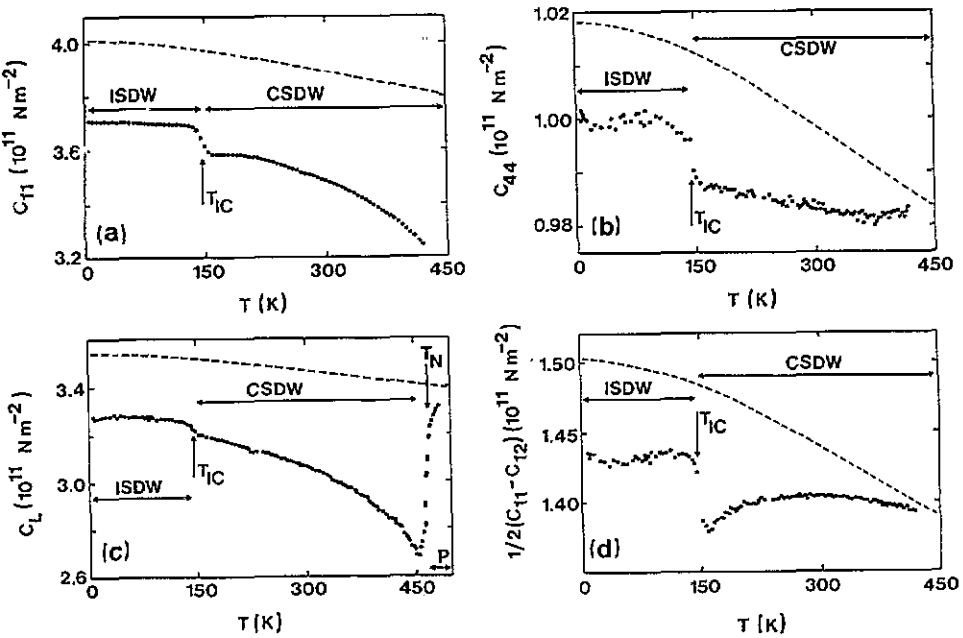

Figure 2. Temperature dependence of the elastic constants of Cr + 0.5 at.% Ru with only every fourth experimental point plotted for clarity. Values depicted for c_{11} in (*a*) were calculated from smooth curves through the data in (*b*), (*c*) and (*d*), since due to very large attenuation for the c_{11} mode, it could not be measured directly as a function of temperature for this crystal. The broken curves give the corresponding elastic constants of a Cr + 5 at.% V crystal.

phase diagrams [1] of these alloy systems and the neutron results of subsection 3.2, the low-temperature anomaly occurs at the spin-flip transition temperature T_{sf} where the transverse (T) ISDW phase transforms to a longitudinal (L) ISDW phase. The high-temperature anomaly occurs at T_N and the third one at T_{IC} where $T_{sf} < T_{IC} < T_N$.

The determination of the transition temperatures for dilute Cr alloys from the anomalies in the magnetoelastic measurements can be problematic. There is presently no theoretical work that predicts the character of the anomalies at T_{sf}, T_{IC} and T_N. Usually [1] electrical resistivity (ρ) against temperature curves of dilute Cr alloys are used to obtain T_N, which is defined at the temperature of the minimum in the $d\rho/dT$–T curves. In the case of Cr–Co alloys, for instance, it was found [12] that the temperature of the minimum on the B–T curves, where B is the bulk modulus, agree with the temperature at the minimum of $d\rho/dT$. For Cr–Al alloys for which the ρ anomaly becomes very weak between 2 and 4 at.% Al, Baran and co-workers [10], on the other hand, found that the temperature at the inflection point to the right of the deep minimum on the B–T curve, corresponds better with T_N, as determined from neutron diffraction measurements. Similarly to the method used in the initial study [5] on the Cr+0.3 at.% Ru crystal, the c_{44}–T curves were used to obtain T_{sf} and T_{IC} for the Cr–Ru and Cr–Re crystals. On these curves T_{sf} was taken at the low-temperature minima for Cr + 0.3 at.% Ru and Cr + 0.3 at.% Re and at the low-temperature inflection point for Cr + 0.5 at.% Re, for which there is no clear minimum in the c_{44} anomaly at low temperatures. The Cr+0.5 at.% Ru crystal does not show a c_{44} anomaly at low temperatures that could be identified with T_{sf}. This crystal shows a very broad minimum in $\frac{1}{2}(c_{11}-c_{12})$ at low temperatures without any evidence from the neutron measurements (subsection 3.2)

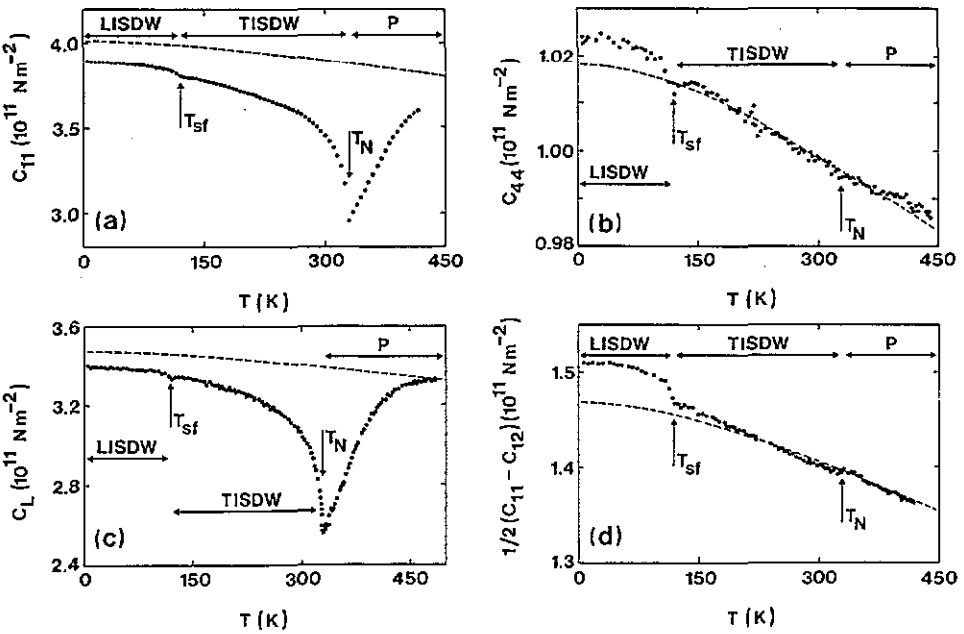

Figure 3. Temperature dependences of the elastic constants of Cr + 0.3 at.% Re with only every fourth experimental point plotted for clarity. c_{11} in (*a*) was calculated from smooth curves through the data in (*b*), (*c*) and (*d*). The non-magnetic behaviour deduced from the temperature dependences of the elastic constants of a Cr + 5 at.% V crystal are indicated by broken curves.

of a spin-flip transition. For all crystals the longitudinal elastic constants show only weak anomalies at T_{sf} or no anomaly at all. T_{IC} was taken on the c_{44}–T curves at the midpoint of the near discontinuity that occurs between T_{sf} and T_N for Cr + 0.3 at.% Ru and at the inflection point of the sharp rise occurring between these two temperatures for Cr + 0.5 at.% Ru and Cr + 0.5 at.% Re. Well defined anomalies are also observed at T_{IC} for c_L and c_{11} of these crystals (figures 1, 2 and 4). However, no anomaly was observed in Cr + 0.3 at.% Re that could be identified with an I–C transition.

For the Cr + 0.3 at.% Ru crystal the peak in the c_{44}–T curve at 402 K corresponds to the inflection point to the right of the sharp minimum in the c_L–T curve and also to the small peak at 400 K in the $\frac{1}{2}(c_{11} - c_{12})$–$T$ curve. This temperature was taken [5] as T_N. T_N was similarly determined at the inflection point to the right of the sharp minimum in the c_L–T curves for the Cr + 0.5 at.% Ru and Cr + 0.5 at.% Re crystals. In the case of Cr + 0.3 at.% Re the high-temperature inflection point to the right of the sharp minimum is, however, not well defined in the results for c_L and T_N was taken at the small maximum near 330 K on the $\frac{1}{2}(c_{11} - c_{12})$–$T$ curve. The transition temperatures as defined above are indicated on figures 1–4 and in table 1. Also indicated in table 1 are the temperatures, T_{min}, of the sharp minimum near T_N in the c_L–T curves. The transition temperatures obtained from the neutron diffraction measurement in subsection 3.2 are also shown in table 1.

Measurements in figures 1–4 were obtained for heating runs only. Hysteresis effects for the Cr–Ru crystals were checked during the neutron diffraction measurements of subsection 3.2. In the case of the Cr + 0.5 at.% Re crystal, however, hysteresis effects near T_{IC} were studied by measuring c_L during both heating and cooling runs and the results are depicted in figure 5. A hysteresis effect of width about 7 K around $T_{IC} \approx 250$ K was

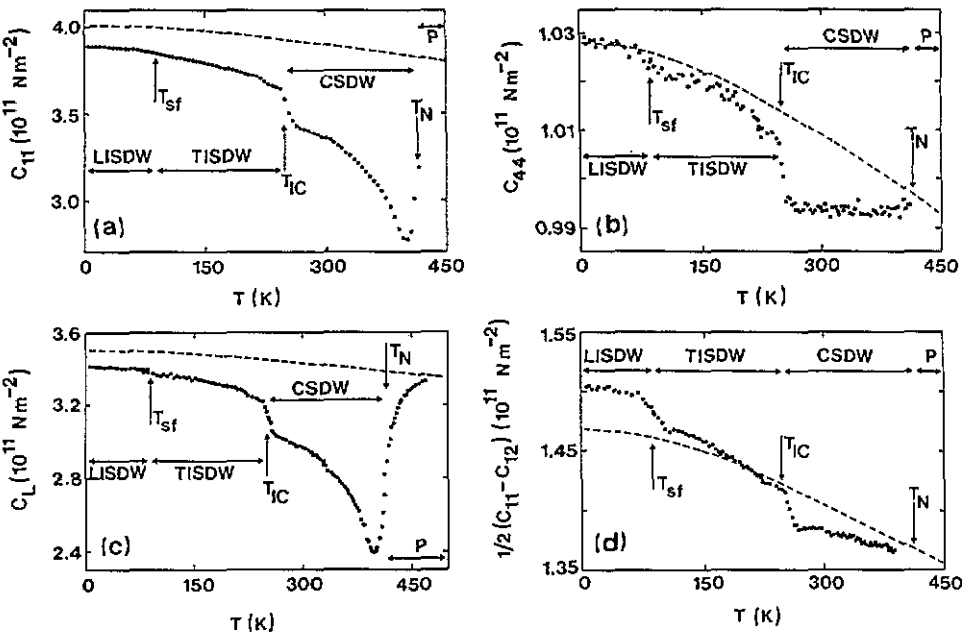

Figure 4. Temperature dependence of the elastic constants of Cr + 0.5 at.% Re with only every fourth experimental point plotted for clarity. c_{11} in (*a*) was calculated from smooth curves through the data in (*b*), (*c*) and (*d*). The broken curves give the corresponding elastic constants of a Cr + 5 at.% V crystal.

observed for this crystal. An interesting feature in figure 5 is the sharp, nearly steplike, change in slope that occurs at approximately 252 K on heating and at 245 K on cooling. The reason for this behaviour is presently unknown.

The broken curves in figure 1 for Cr + 0.3 at.% Ru and in figure 3 for Cr + 0.3 at.% Re represent the non-magnetic behaviour of the crystals. The temperature dependence of the non-magnetic behaviour is taken to be represented by that of the corresponding elastic constant of a Cr + 5 at.% V single crystal [13] which remains paramagnetic at all temperatures. The corresponding curves of Cr + 5 at.% V in figures 1 and 3 were slightly translated up or down to coincide with the Cr–Ru and Cr–Re measurements at the highest temperatures. This procedure gives non-magnetic behaviour that corresponds well with the observed temperature dependence above T_N (compare for instance the broken curves and the actual measurements of c_{44} and $\frac{1}{2}(c_{11} - c_{12})$, which show very small magnetic anomalies, for Cr + 0.3 at.% Re in figure 3). This correspondence was also found in Cr–Si single crystals for which T_N lies well below room temperature, so that the dependence of the corresponding elastic constants of Cr + 5 at.% V and Cr–Si, could be compared over a larger temperature interval above T_N [14]. These latter results in a sense justify the above procedure to obtain the non-magnetic behaviour of the Cr–Ru and Cr–Re alloys. The magnetic contribution to the appropriate elastic constant in figures 1 and 3 at each temperature is given by the difference between the broken curve and the measured value at that temperature. The above procedure was not carried out for the Cr + 0.5 at.% Ru and Cr + 0.5 at.% Re crystals, as measurements could not be done to high enough temperatures above T_N, due to transducer bond failure, for a reliable back extrapolation. For these two crystals the temperature dependence of the actual measurements [13] on the Cr + 0.5 at.%

Table 1. Magnetic transition temperatures T_{sf}, T_{IC} (on heating), T_{CI} (on cooling) and T_N for Cr + 0.3 at.% Ru, Cr + 0.5 at.% Ru, Cr + 0.3 at.% Re and Cr + 0.5 at.% Re single crystals as determined from ultrasonic and neutron diffraction measurements. Also given is the temperature, T_{min}, of the deep minimum in the c_L–T curve.

Sample	$T_{sf}(K)$		$T_{IC}(K)$		$T_{CI}(K)$		$T_N(K)$		$T_{min}(K)$
	Ultrasonics	Neutrons	Ultrasonics	Neutrons	Ultrasonics	Neutrons	Ultrasonics	Neutrons	Ultrasonics
0.3 at.% Ru	85 ± 5	75 ± 9	257 ± 5	255 ± 4	—	240 ± 4	402 ± 5	406 ± 5	394 ± 5
0.5 at.% Ru	—	—	146 ± 8	143 ± 6	—	92 ± 6	465 ± 8	462 ± 5	454 ± 5
0.3 at.% Re	119 ± 8	—	—	—	—	—	328 ± 8	—	329 ± 5
0.5 at.% Re	87 ± 9	—	250 ± 9	—	—	—	414 ± 8	—	396 ± 5

V crystal are however shown in figures 2 and 4 for comparison purposes. The temperature dependence of the magnetic contributions Δc_{11}, Δc_{44} and $\Delta\frac{1}{2}(c_{11}-c_{12})$ for Cr + 0.3 at.% Ru and Cr + 0.3 at.% Re are shown in figures 6 and 7.

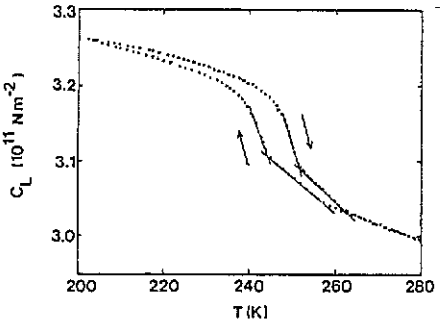

Figure 5. Temperature dependence of $c_L = \frac{1}{2}(c_{11} + c_{12} + 2c_{44})$ for Cr+0.5 at.% Re near T_{IC} during heating and cooling runs.

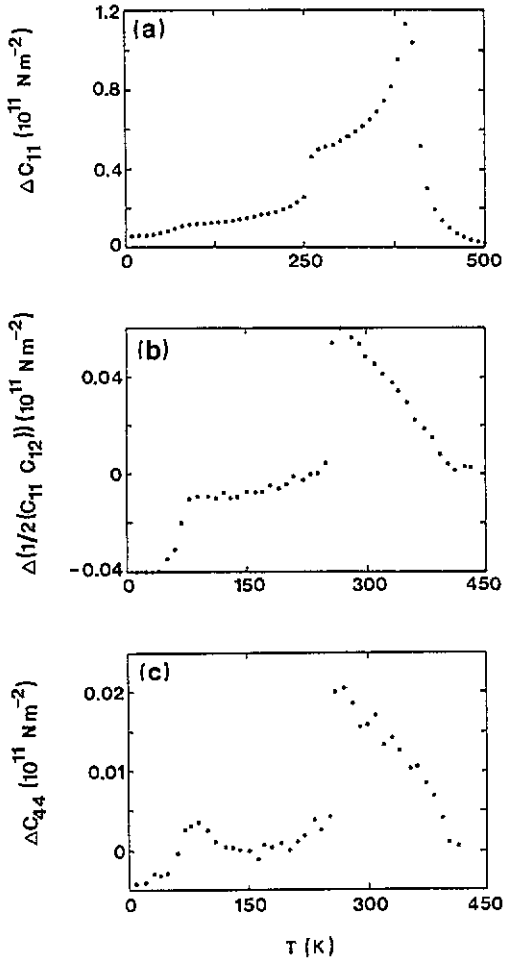

Figure 6. Temperature dependence of the magnetic contributions Δc_{11}, Δc_{44} and $\Delta\frac{1}{2}(c_{11}-c_{12})$ for Cr + 0.3 at.% Ru.

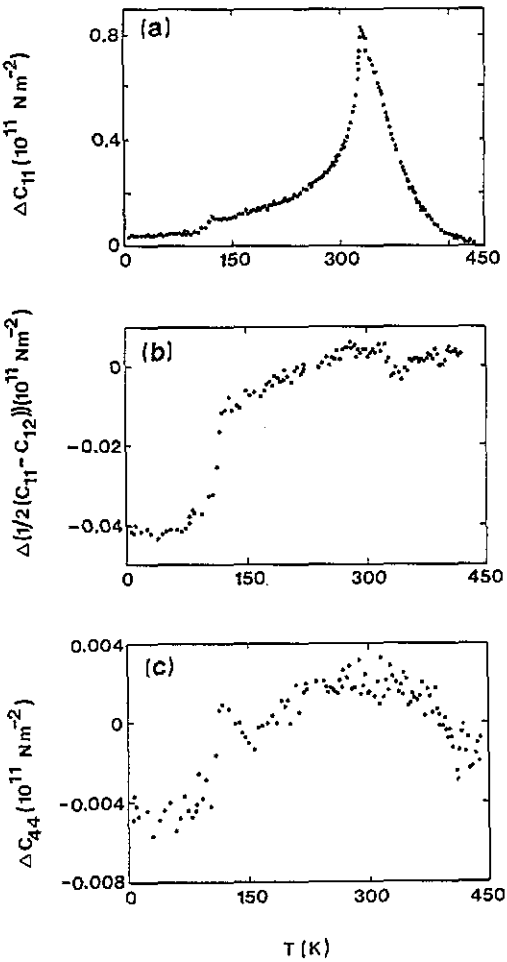

Figure 7. Temperature dependence of the magnetic contributions Δc_{11}, Δc_{44} and $\Delta\frac{1}{2}(c_{11}-c_{12})$ for Cr + 0.3 at.% Re.

3.2. Neutron diffraction

3.2.1. Cr + 0.3 at.% Ru crystal. Figures 8(*a*), (*b*) and (*c*) show the neutron diffraction patterns for the Cr + 0.3 at.% Ru crystal at temperatures of 262.3 K, 152.3 K and 44.3 K, representative of the three magnetic phases of the crystal. The results were obtained using ω scans through the (010) reciprocal lattice point while the [001] direction of the crystal was perpendicular to the plane of the diffractometer. The pattern at 262.3 K consists of a single peak at (010) and is characteristic of the CSDW phase. At 152.3 K two peaks are observed left and right of the (010) position, at the $(+\delta, 1, 0)$ and $(-\delta, 1, 0)$ reciprocal lattice points respectively, while the central peak now has a structure which is due to the superposition of different magnetic satellites, presumably $(0, 1 \pm\delta, 0)$ and $(0, 1, \pm\delta)$ satellites. This is characteristic of the TISDW phase [15]. The pattern at 44.3 K is characteristic [15] of the LISDW phase and has three diffraction peaks, two outermost satellites at $(\pm\delta, 1, 0)$ and a central peak consisting of the superposition of $(0, 1, \pm\delta)$ satellites.

Figure 9(*a*) shows at each temperature the sum of the integrated neutron intensities of the $(\pm\delta, 1, 0)$ satellites (see figures 8(*b*) and (*c*)), obtained during both cooling and heating runs from 12–300 K. The transition temperatures $T_{sf} = 75 \pm 9$ K, T_{IC} (on heating) $= 255 \pm 4$ K and T_{CI} (on cooling) $= 240 \pm 4$ K are shown in the figure and are given in

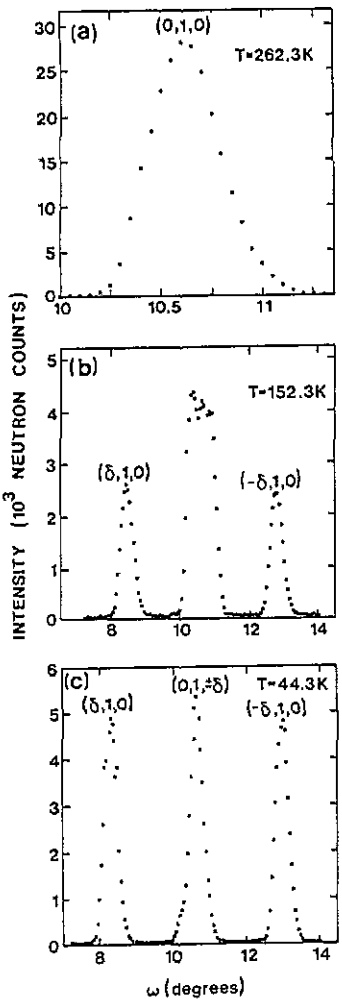

Figure 8. Neutron diffraction patterns obtained for the Cr + 0.3 at.% Ru crystal during ω scans through the (010) reciprocal lattice point. (*a*) $T_{IC} < T < T_N$, (*b*) $T_{sf} < T < T_{IC}$ and (*c*) $T < T_{sf}$. The central peak intensity near (010) in figure (*b*) is a superposition of satellites as discussed in the text.

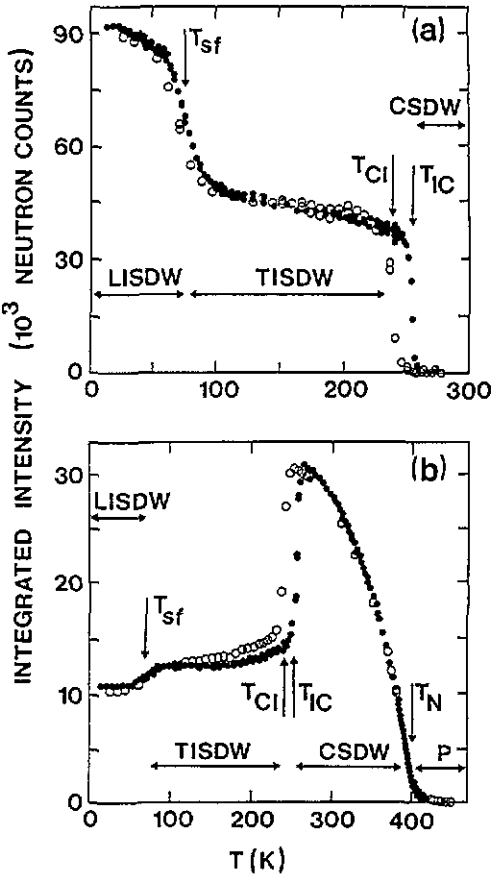

Figure 9. (*a*) Temperature dependence of the sum of the integrated neutron intensities of the $(\pm\delta, 1, 0)$ satellites for Cr + 0.3 at.% Ru of figures 8(*b*) and (*c*): open circles, cooling run; full circles, heating run. (*b*) Temperature dependence of the integrated intensities of the (010) peak for Cr + 0.3 at.% Ru in figure 8(*a*) from 260 K to 500 K and that of the central peaks of figures 8(*b*) and (*c*) below 260 K. Cooling run: open circles; heating run: full circles.

table 1. They were taken at the midpoints (T_{IC} and T_{CI}) or inflection point (T_{sf}) of the sharp rises that occur near these temperatures. The ISDW–CSDW phase transition in figure 9(*a*) near 250 K is nearly discontinuous and shows hysteresis of width 15 K. This is characteristic of a first-order transition which was recently also confirmed in high-pressure ultrasonic studies [16, 17] on this crystal. The transition at T_{sf} in figure 9(*a*), on the other hand, seems more continuous with smaller hysteresis. The possibility that inhomogeneities are responsible for the continuous transition at T_{sf} is ruled out by the fact that the ISDW–CSDW transition in figure 9(*a*) is fairly sharp, thereby indicating a crystal of rather good homogeneity.

The integrated intensities of the (010) peak (see figure 8(*a*)) in the temperature range 260–500 K and that of the central peaks (see figures 8(*b*) and (*c*)) below 260 K, are shown as a function of temperature for Cr + 0.3 at.% Ru in figure 9(*b*). An interesting feature in this figure is the fact that, although the hysteresis effects are absent in the CSDW phase above $T_{IC} = 255 \pm 4$ K, it persists in the ISDW phase down to about $T = 100$ K, well below $T_{CI} = 240 \pm 4$ K. This persistence of hysteresis effects below T_{CI} in the Cr + 0.3 at.% Ru crystal is also found in the behaviour of the elastic constant c_L of Cr + 0.5 at.% Re below T_{IC} in figure 5.

The transition at T_N in figure 9(*b*) is continuous without any hysteresis to within the experimental accuracy.

3.2.2. Cr + 0.5 at.% Ru. Neutron diffraction patterns for the Cr + 0.5 at.% Ru crystal are shown in figure 10(*a*) and (*b*) at 210.0 K and 51.2 K, representative of the following two magnetic phases. For the higher-temperature phase (figure 10(*a*)) a single peak is observed at the reciprocal lattice point (010), as is expected for the CSDW phase. For the lower-temperature phase (figure 10(*b*)) two weak satellites, characteristic of the ISDW phase, develop at the ($\pm\delta$, 1, 0) positions. It is further observed in figure 10(*b*) that the intensity of the central peak diminishes only moderately, without any sign of the magnetic satellites characteristic of the TISDW state that should be superimposed on it (see also figure 8(*b*)). Evidence for the presence of a TISDW phase in this crystal at low temperatures, is indirectly obtained from the temperature behaviour of the elastic constants thereof. The longitudinal constant c_L, for instance, of both Cr + 0.3 at.% Ru and Cr + 0.5 at.% Ru behaves very similarly at low temperatures, as shown in figures 1 and 4. Both crystals show a jump, at about 255 K for Cr+0.3 at.% Ru and at about 143 K for Cr+0.5 at.% Ru, when cooled from room temperature down to 4 K. As the neutron measurements on the 0.3 at.% Ru crystal show that this jump is associated with a CSDW–TISDW phase transition on cooling, we also assume this to be the case for the 0.5 at.% Ru crystal.

Figure 11(*a*) shows at each temperature the sum of the integrated neutron intensities of the ($\pm\delta$, 1, 0) satellites (see figure 10(*b*)), obtained for the Cr + 0.5 at.% Ru crystal during both cooling and heating runs from 12–300 K. The temperature dependence of the integrated neutron intensity of the central peak at (010) of figure 10(*a*), is shown in figure 11(*b*) in the temperature range 12–500 K. Large hysteresis effects of width about 55 K are observed for this crystal with a 'jump-like' behaviour at T_{IC} and T_{CI} in figure 11(*a*) and (*b*), making the ISDW-CSDW transition first order as for Cr + 0.3 at.% Ru. The transition from the CSDW to ISDW phase for Cr + 0.5 at.% Ru seems to be incomplete as evidenced by only a moderate drop in intensity below T_{IC} in figure 11(*b*). Mixed ISDW/CSDW states possibly exist in the low-temperature regime as were previously reported for other dilute Cr alloys [18].

The CSDW–P transition at T_N is continuous without hysteresis effects, as for Cr+0.3 at.% Ru. No TISDW–LISDW transition was observed in the Cr+0.5 at.% Ru crystal down to 12 K. Transition temperatures T_{IC}, T_{CI} and T_N were defined as for the Cr + 0.3 at.% Ru crystal and are also shown in table 1.

3.3. Critical behaviour

The critical behaviour of the two Cr–Ru crystals was analysed in a manner similar to that previously used [10] in a study on Cr–Al crystals. From subsection 3.2, the magnetic transition at T_N is continuous for both the Cr + 0.3 at.% Ru and Cr + 0.5 at.% Ru crystals, being a CSDW-P transition in both cases. Neglecting extinction effects as previously [10], and taking the intensity, I_m, of the magnetic Bragg reflections to be proportional

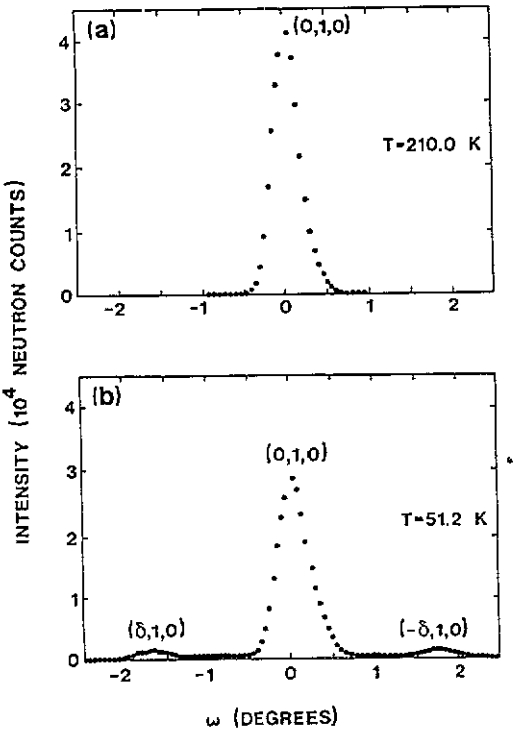

Figure 10. Neutron diffraction patterns obtained for the Cr + 0.5 at.% Ru crystal during ω scans through the (010) reciprocal lattice point. (*a*) $T_{IC} < T < T_N$ and (*b*) $T < T_{IC}$.

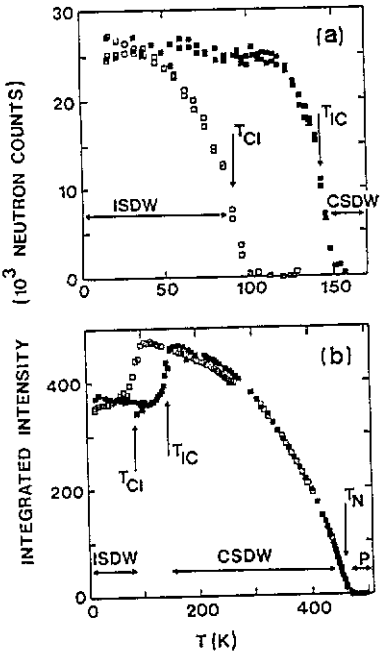

Figure 11. (*a*) Temperature dependence of the sum of the integrated neutron intensities of the $(\pm\delta, 1, 0)$ satellites of figure 10(*b*) for Cr + 0.5 at.% Ru: open squares, cooling; full squares, heating. (*b*) Temperature dependence of the integrated intensities of the (010) peak for Cr + 0.5 at.% Ru as obtained from figures 10(*a*) and 10(*b*): open squares, cooling; full squares, heating.

to $m^2 = M^2(T)/M^2(0)$, where $M(T)$ is the spontaneous sublattice magnetization of the CSDW phase, the integrated neutron intensity, I, near T_N is written as [10]

$$I = I_m + I_{c+} + I_{c-} = At_-^{2\beta} + C_+t_+^{-\gamma} + C_-t_-^{-\gamma}. \quad (1)$$

In this equation $t_\pm = \pm(T - T_N)/T_N$, where the + and − signs correspond to $T > T_N$ and $T < T_N$ respectively, the critical exponent β describes the sublattice magnetization $m \sim t_-^\beta$ and, in accordance with the scaling hypothesis, γ is taken the same for $T > T_N$ and $T < T_N$ [19]. C_+ and C_- are related [20] through

$$\frac{C_+}{C_-} = \frac{\gamma}{\beta}\left(\frac{(1-2\beta)\gamma}{2(\gamma-1)\beta}\right)^{\gamma-1}. \quad (2)$$

The parameters β, T_N and γ were determined from the above equations by a least-squares fit analysis as previously described for Cr–Al alloys [10]. It was found that the effect of critical scattering in (1) is small. Including or excluding critical scattering ($\gamma = 1.4$) in the analysis for Cr + 0.5 at.% Ru gives respectively $\beta = 0.40$ and $\beta = 0.39$. In the previous study [10] on Cr–Al alloys it was similarly found that β was not significantly affected by critical scattering. For Cr + 0.3 at.% Ru the analysis was done by including only the term I_m in (1) to obtain $\beta = 0.29$.

The values $\beta = 0.40$ for Cr + 0.5 at.% Ru and $\beta = 0.29$ for Cr + 0.3 at.% Ru disagree with the mean-field-like value of $\beta = 0.5$ found for Cr–Al alloys [10]. We do not know the reason for this difference in behaviour of the Cr–Ru and Cr–Al systems, but we mention that the three-dimensional Heisenberg model [21] gives $\beta = 0.37$ while the three-dimensional Ising model [19] gives $\beta = 0.3125$.

4. Discussion

In table 1, values of T_{sf}, T_{IC} and T_N obtained from both ultrasonic and neutron diffraction measurements during heating runs on Cr + 0.3 at.% Ru and Cr + 0.5 at.% Ru, compare reasonably well within the experimental error. The procedure used in subsection 3.1 to obtain these temperatures from the ultrasonic measurements thus seems to be acceptable. In previous studies [22, 23] on polycrystalline Cr+0.3 at.% Ru, Cr+0.5 at.% Ru, Cr+0.3 at.% Re and Cr+0.5 at.% Re, T_N was taken at the high-temperature minimum in the B–T curves. The present study shows that the inflection point to the right of the minimum on these curves, agrees better with neutron results. In the polycrystalline measurements [22, 23] anomalies were observed in B and in the shear constant, G, at T_{IC} (on heating) for Cr + 0.3 at.% Ru and Cr + 0.5 at.% Ru but not for Cr + 0.3 at.% Re and Cr + 0.5 at.% Re, while T_{sf} was not observed in any of these polycrystals. The present measurements on the single crystals, however, show well defined anomalies in the temperature dependence of the elastic constants at all three transition temperatures. T_{IC} obtained [22] during heating runs from the low-temperature minimum in dB/dT for polycrystalline Cr+0.3 at.% Ru and Cr+0.5 at.% Ru, do not compare well with the single crystalline T_{IC}. For the former polycrystal it is about 13 K higher and for the latter about 60 K higher than the value of T_{IC} obtained for the single crystals. It is difficult to explain this discrepancy, but it may be noted that the I–C transition on the B–T and G–T curves of the polycrystals is smeared out over about 75 K while it is nearly discontinuous in the elastic constant-temperature curves of the single crystals.

The temperature dependence of the elastic constants and thermal expansion of Cr and dilute Cr alloys is often analysed in terms of a thermodynamic model [1, 24] developed from an analysis by Testardi [25]. The assumptions of the model are [26]: (i) the magnetic free energy, ΔF, is separable from the total free energy, (ii) the volume-strain

terms in ΔF dominate the shear strain effects, (iii) ΔF is a function of a single volume-dependent characteristic temperature and, (iv) for small strain the characteristic temperature is approximately a linear function in strain. In pure Cr and in some dilute Cr–alloys the effects of shear strain are very small and the thermodynamic model was applied successfully to Cr [27], Cr–Mo [28], Cr–Fe [29] and Cr–Al [10] alloys, indicating that the above assumptions are met for these cases. The Cr+0.3 at.% Re crystal remains in the ISDW phase below T_N and exhibits magnetic contributions to the shear constants, c_{44} and $\frac{1}{2}(c_{11} - c_{12})$, that are negligible compared to that of c_{11} and c_L. This crystal thus seems appropriate for applying the thermodynamic model. For the Cr + 0.5 at.% Re, Cr + 0.3 at.% Ru and Cr + 0.5 at.% Ru crystals that show I–C transitions, shear effects remain very small in the ISDW phases but become relatively larger in their CSDW phases. It is however still relatively small compared to that of c_{11} and c_L in the CSDW phase (see figures 1, 2 and 4). For Cr + 0.3 at.% Ru, for instance, the maximum magnetic contribution to c_{44} in the CSDW phase is approximately 2% to c_{44} and 4% to $\frac{1}{2}(c_{11} - c_{12})$, while it is approximately 50% to B. The thermodynamic model is therefore also expected to be applicable, to a good approximation, in the CSDW phases of the Cr–Re and Cr–Ru crystals. The analysis will give information on the usefulness of applying the thermodynamic model to all magnetic phases of dilute Cr alloys.

The magnetic free energy is given by [27]

$$\Delta F(t, \omega) = \phi(w) f[t(\omega)]$$

where $t = T/T_0(w)$, with $T_0(w)$ a characteristic temperature. For $T \to T_N$ from below or from above, ϕ is assumed [27] to be constant, independent of the volume strain w, and $T_0(w) = T_N(w)$. At lower temperatures ϕ depends on w. Taking $f(t) = (1 - t^2)^2$ in this case, as was previously done for Cr alloys [1, 29], and assuming $T_0(w)$ to be linear in w [27], one obtains [29]

$$\Delta B = b_0 + b_1 t^2 + b_2 t^4 \tag{3}$$

$$\Delta w = a_0 + a_1 t^2 + a_2 t^2 \tag{4}$$

for the magnetic contributions to the bulk modulus, B, and magnetovolume Δw, respectively.

Constants (b_0, b_1, b_2) and (a_0, a_1, a_2) contain ϕ, its first and second derivatives to strain, as well as T_0 and its first and second derivatives to strain, and are given by (3) and (5) of [29]. Measurements of (a_0, a_1, a_2) and (b_0, b_1, b_2) allow for a determination of $\mathrm{d}\ln\phi/\mathrm{d}w$ and $\mathrm{d}\ln T_0/\mathrm{d}w$ through the equations [29]

$$\mathrm{d}\ln\phi/\mathrm{d}w = -4[(a_1/a_0) + 2(a_2/a_0)]^{-1}(\mathrm{d}\ln T_0/\mathrm{d}w) \tag{5}$$

$$= \frac{8}{\Gamma_0}\left(\frac{\mathrm{d}\ln T_0}{\mathrm{d}w}\right)^2\left(\frac{b_1}{b_0} + \frac{b_2}{b_0} + 1\right)^{-1} \tag{6}$$

$$\mathrm{d}\ln T_0/\mathrm{d}w = -\frac{\Gamma_0}{16}\left(5\frac{b_1}{b_0} + 3\frac{b_2}{b_0} + 7\right) \tag{7}$$

where

$$\Gamma_0 = -\phi''/\phi' = b_0/Ba_0. \tag{8}$$

In the Steinemann [1, 30] application of the thermodynamic model, $T_0(w) \equiv T_N(w)$ at all $T < T_N$. For Cr and dilute Cr alloys, the magnetovolume can also be written [1, 10, 27] in terms of the magnetization as

$$\Delta w(T) = C(T)\langle M^2(T)\rangle \tag{9}$$

where $\langle M^2(T)\rangle$ is the mean square magnetic moment and the magnetoelastic coupling constant, C(T), is taken to be temperature dependent. Neglecting spin fluctuations or rotations below T_N, $\langle M^2(T)\rangle = M_0^2(T)/2$ for the ISDW phase and $\langle M^2(T)\rangle = M_0^2(T)$ for the CSDW phase [1], where $M_0(T)$ is the peak moment. In (9) [10, 31]

$$C(T) = C(0)[1 + \zeta(T/T_N)^2] \tag{10}$$

$$\langle M^2(T)\rangle = \langle M^2(0)\rangle[1 + \alpha(T/T_N)^2 + \delta(T/T_N)^4]. \tag{11}$$

From (9)

$$\Delta w(t)/\Delta w(0) = (1 + \zeta t^2)\langle M^2(t)\rangle/\langle M^2(0)\rangle \tag{12}$$

where $t = T/T_N$. Equation (4) for Δw then also follows from (11) and (12) if $T_0(w)$ is taken to be proportional to $T_N(w)$. For the rest of the discussion we take $T_0 = T_N$, as was done in the Steinemann [30] application of the thermodynamic model and was found [29] to be a reasonably good approximation in Cr–Fe alloys, for which (3) and (4) were found to fit the experimental data rather well from low temperatures to temperatures close to T_N.

The above theory was used to analyse the results obtained for the Cr + 0.3 at.% Re and Cr + 0.5 at.% Ru crystals. As the former remains in the ISDW phase at all $T < T_N$, and the temperature range in which the CSDW phase exists in the latter is the largest of the four alloys studied, these two crystals are best suited for this purpose.

Figure 12(*a*) and (*b*) show ΔB as a function of temperature below T_N for Cr + 0.5 at.% Ru and Cr + 0.3 at.% Re together with the best fits of (3) to the results. For Cr + 0.5 at.% Ru for which B could not be measured to temperatures well above T_N, ΔB was obtained by subtracting the measured B values directly from the B values of Cr + 5 at.% V as given by Alberts [13]. This procedure will not affect b_1 and b_2 of equation (3) but only b_0, for which the estimated error, caused by not translating the B–T curve of Cr + 5 at.% V slightly up or down, as was done for Cr + 0.5 at.% Ru, is about 10%. The fits of (3) to the data in figure 12(*a*) and (*b*) are rather good, even up to temperatures fairly close to T_N. The fitting parameters (b_0, b_1, b_2) are shown in table 2 together with the experimental errors obtained by the least-squares fitting procedure.

Table 2. Values of b_0, b_1 and b_2 in the expression $\Delta B = b_0 + b_1 t^2 + b_2 t^2$, where $t = T/T_N$, obtained for the Cr + 0.5 at.% Ru and Cr + 0.3 at.% Re crystals by a least squares fit to the experimental data.

Sample	$b_0(10^{11}\mathrm{Nm}^{-2})$	$b_1(10^{11}\mathrm{Nm}^{-2})$	$b_2(10^{11}\mathrm{Nm}^{-2})$
0.5 at.% Ru	0.276 ± 0.010	0.220 ± 0.020	0.225 ± 0.023
0.3 at.% Re	0.10 ± 0.01	0.090 ± 0.01	0.22 ± 0.02

The magnetic moment could not be obtained from our neutron diffraction measurements in the ISDW phases of the alloys, as this requires in principle well resolved neutron

intensity measurements of all magnetic satellites around the (010) position. For the CSDW phase only a single peak is observed at the (010) position and provided that no changes in domain structure occurs [32], measurement of the temperature dependence of the integrated intensity reliably gives the behaviour of the reduced sublattice magnetization m. If extinction effects [10] are negligible, the integrated intensity $I(T) \propto m^2(T)$. As shown in figure 13(*a*) the measured intensities for the CSDW phase of the Cr + 0.5 at.% Ru crystal, is well fitted by an equation of the form $I(T) = C_0 + C_1T^2 + C_2T^4$, which gives $M^2(T)/M^2(0) = 1+k(T/T_N)^2+\ell(T/T_N)^4$ with $k = -(0.25\pm0.01)$ and $\ell = -(0.72\pm0.02)$.

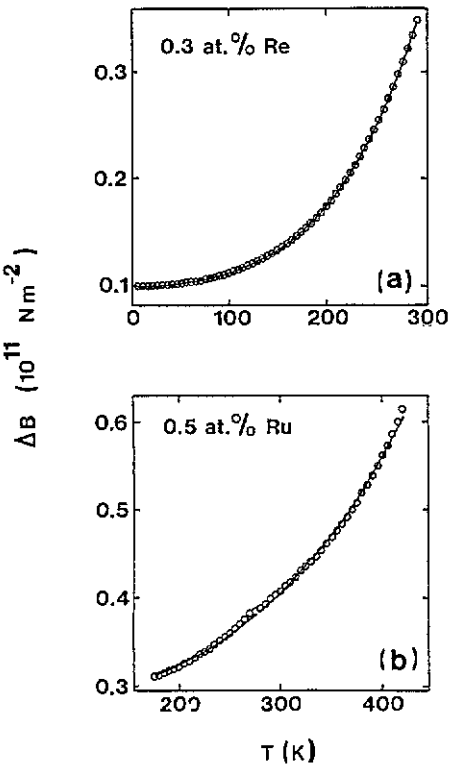

Figure 12. The magnetic contribution, ΔB, to the bulk modulus, B, as a function of temperature for (*a*) Cr + 0.3 at.% Re and (*b*) Cr + 0.5 at.% Ru in the CSDW phase. The full curves are the best fit of the equation $\Delta B = A_0 + A_1T^2 + A_2T^4$ to the data.

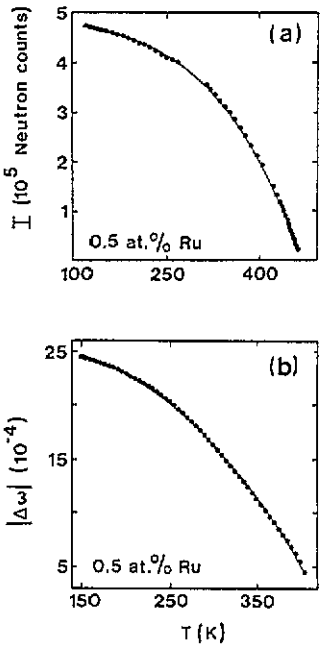

Figure 13. (*a*) Integrated neutron intensity, I, of the (010) peak of the CSDW phase of Cr + 0.5 at.% Ru as a function of temperature. The full curve is the best fit of the equation $I(T) = C_0 + C_1T^2 + C_2T^4$ to the data. (*b*) The magnetovolume, $\Delta\omega$, of polycrystalline Cr + 0.5 at.% Ru as a function of temperature. The full curve is the best fit of the equation $|\Delta\omega| = D_0 + D_1T^2 + D_2T^4$ to the data.

The magnetovolume, $\Delta w(T)$, of polycrystalline Cr + 0.5 at.% Ru was measured by Alberts and Lourens [22]. Figure 13(*b*) shows $\Delta w(T)$ as a function of temperature obtained from their work, together with the best fit of (4) to the data. The fit is fairly good, giving $a_0 = -(27.10 \pm 0.01) \times 10^{-4}$, $a_1 = (0.18 \pm 0.01) \times 10^{-4}$ and $a_2 = (9 \pm 1) \times 10^{-4}$ using $T_N = 435$ K for the polycrystalline $\Delta w(T)$ results. It is now possible to test the validity of (12) for the Cr + 0.5 at.% Ru crystal. Figure 14 shows a graph of $\Delta w(t)/\Delta w(0)$ as a function of $[1 - 0.3t^2]M^2(t)/M^2(0)$ for this crystal in its CSDW phase. Equation (12) fits

the experimental results fairly well with $\zeta = -0.3$. The only other dilute Cr alloy system for which ζ was determined previously is the Cr–Al system. Baran and co-workers [10] obtained $\zeta = +0.52$ for Cr + 2.6 at.% Al giving, surprisingly, an increase of $C(T)$ with increasing T. For Cr + 0.5 at.% Ru, however, $C(T)$ decreases with increasing temperature, as expected intuitively.

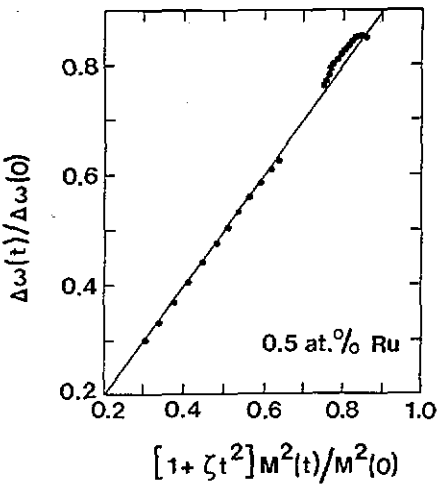

Figure 14. $\Delta\omega(t)/\Delta\omega(0)$ as a function of $[1 + \zeta t^2]M^2(t)/M^2(0)$ where $\zeta = -0.3$, for Cr + 0.5 at.% Ru and $t = T/T_N$. The full curve is the theoretical behaviour expected from (12).

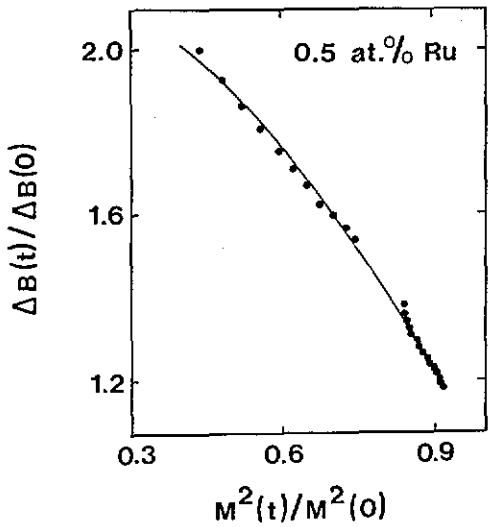

Figure 15. $\Delta B(t)/\Delta B(0)$ as a function of $M^2(t)/M^2(0)$ for Cr + 0.5 at.% Ru where $t = T/T_N$. The full curve is the best fit of the equation $\Delta B(t)/\Delta B(0) = E_0 + E_1 M^2(t)/M^2(0) + E_2 M^4(t)/M^4(0)$.

In Steinemann's [30] thermodynamic analysis, which is often used [1] for Cr and its alloys, $\phi \propto [T_N(w)]^4$ and $M^2(t) = M^2(0)(1 - t^2)$. This gives

$$\Delta B(t)/\Delta B(0) = [(3 - t^2)/3(1 - t^2)][M^2(t)/M^2(0)] \tag{13}$$

where T_N is assumed to be linear in strain.

Equation (13) does not fit the results for the Cr + 0.5 at.% Ru crystal in its CSDW phase, pointing to possible incompleteness of the Steinemann approach. The $\Delta B(T)/\Delta B(0)$ data for this crystal are instead fitted reasonably well by the equation

$$\Delta B(t)/\Delta B(0) = (2.23 \pm 0.02) - (1.4 \pm 0.1)M^2(t)/M^2(0) + (0.14 \pm 0.09)M^4(t)/M^4(0) \tag{14}$$

as shown in figure 15.

The terms $d\ln T_N/dw$ and $d\ln\phi/dw$ were calculated for Cr + 0.5 at.% Ru using (5)–(8). The calculation gives $d\ln\phi/dw = (14 \pm 13)$ and $d\ln\phi/dw = (122 \pm 11)$ as obtained from (5) and (6), respectively, and $d\ln T_N/dw = (48 \pm 4)$. The values of $d\ln\phi/dw$ obtained for the Cr + 0.5 at.% Ru crystal are of the same order of magnitude as obtained for dilute Cr–Fe alloys [29]. The pressure dependence of T_N was measured directly by Jayaraman and co-workers [33] for polycrystalline Cr + 0.3 at.% Ru and Cr + 0.6 at.% Ru. From their results a value $\ln T_N/dw \simeq 58$ is obtained by interpolation for Cr + 0.5 at.% Ru. This value compares fairly well with the value $d\ln T_N/dw = 48$ obtained from the magnetoelastic measurements in the present study on the Cr + 0.5 at.% Ru single crystal.

5. Conclusions

It is concluded that the ISDW-CSDW and CSDW-ISDW magnetic transitions in dilute Cr–Ru and Cr–Re single crystals are first-order transitions while the CSDW-P and ISDW-P transitions are of second order. The thermodynamic model predicts the temperature dependence of the magnetic contributions to the bulk modulus, in both the ISDW and CSDW phases of these alloys, reasonably well. However, it fails to give the correct relationship between these contributions and the magnetization of the alloys, pointing to shortcomings in the thermodynamic model.

Acknowledgments

Financial aid from the Foundation for Research Development is acknowledged, as well as technical assistance from T Germishuyse and S I Wagener.

References

[1] Fawcett E, Alberts H L, Galkin V Yu, Noakes D R and Yakhmi J V 1993 *Rev. Mod. Phys* submitted for publication
[2] Mikke K and Jankowska J 1980 *J. Phys. F: Met. Phys.* **10** L159
[3] Lebech B and Mikke K 1972 *J. Phys. Chem. Solids* **33** 1651
[4] Mikke K and Jankowska 1979 *J. Magn. Magn. Mater.* **14** 280
[5] Alberts H L and Boshoff A H 1992 *J. Magn. Magn. Mater.* **104–7** 2031
[6] Papoular R, Debray D and Arajs S 1981 *J. Magn. Magn. Mater.* **24** 106
[7] Bohlmann M and Alberts H L 1970 *J. Phys. E: Sci. Instrum.* **3** 779
[8] Nishihara Y, Yamaguchi Y, Kohara T and Tokumoto M 1985 *Phys. Rev.* B **31** 5775
[9] Nishihara Y, Yamaguchi Y, Tokumoto M, Takeda K and Fukamichi K 1986 *Phys. Rev.* B **34** 3446
[10] Baran A, Alberts H L, Strydom A M and du Plessis P de V 1992 *Phys. Rev.* B **45** 10473
[11] Greenwood P H and du Plessis P du V 1985 *Phys. Stat. Sol. (b)* **127** K19
[12] Alberts H L and Lourens J A J 1983 *J. Phys. F: Met. Phys.* **13** 873
[13] Alberts H L 1990 *J. Phys.: Condens. Matter* **2** 9707
[14] Anderson R A, Alberts H L and Smit P 1993 *J. Phys.: Condens. Matter* in press
[15] Bastow T J and Street R 1966 *Phys. Rev.* **141** 510
[16] Alberts H L, Ford P J, Rahdi H and Saunders G A 1992 *J. Phys.: Condens. Matter* **4** 2793
[17] Cankurtaran M, Saunders G A, Wang Q, Ford P J and Alberts H L 1992 *Phys. Rev.* B **46** 14370
[18] Booth J G, Costa M M R, Rodriguez-Carjaval J and Paixao J A 1992 *J. Magn. Magn. Mater.* **104–7** 735
[19] Stanley H E 1971 *Phase Transitions and Critical Phenomena* (Oxford: Claredon)
[20] Schofield P, Litster J D and Ho J T 1969 *Phys. Rev. Lett.* **23** 1098
[21] Fisher M E 1974 *Rev. Mod. Phys.* **46** 597
[22] Alberts H L and Lourens J A J 1988 *J. Phys. F: Met. Phys.* **18** L213, and private communication
[23] Alberts H L 1989 *Physica* B **161** 87
[24] Fawcett E and Alberts H L 1992 *J. Phys.: Condens. Matter* **4** 613
[25] Testardi L R 1975 *Phys. Rev.* B **12** 3849
[26] Fawcett E, Acet M, Shiga M and Wasserman E F 1992 *Phys. Rev.* B **45** 2180
[27] Fawcett E 1989 *J. Phys.: Condens. Matter* **1** 203
[28] Fawcett E and Alberts H L 1990 *J. Phys.: Condens. Matter* **2** 6251
[29] Alberts H L and Lourens J A J 1992 *J. Phys.: Condens. Matter* **4** 3835
[30] Steinemann S G 1978 *J. Magn. Magn. Mater.* **7** 84
[31] Alberts H L and Lourens J A J 1984 *Phys. Rev.* B **29** 5279
[32] Werner S A, Arrott A and Kendrick H 1967 *Phys. Rev.* **155** 528
[33] Jayaraman A, Rice T M and Bucher E 1970 *J. Appl. Phys.* **41** 869